

Structure–Solubility Relationship of CO Dispersion in Model Hydrocarbon Liquids and Heavy Oil Fractions

He Liu,* Shiguang Fan, Jian Wang, Hao Liu, Aijun Guo, Kun Chen, Zongxian Wang, and Litao Wang

Cite This: *ACS Omega* 2021, 6, 23317–23328

Read Online

ACCESS |



Metrics & More

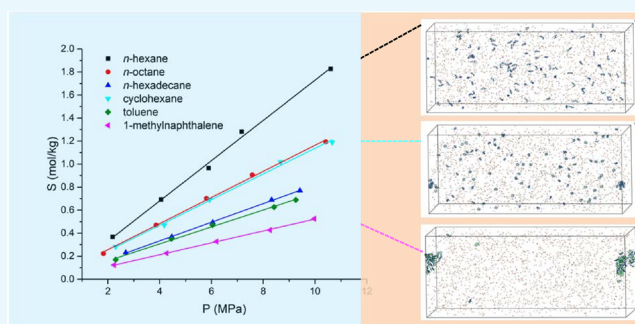


Article Recommendations



Supporting Information

ABSTRACT: The solubility of CO in heavy oils is an important parameter for designing and optimizing the partial upgrading process of heavy oil under CO/syngas and water. To study the structure–solubility relationship of CO dispersion in organic liquids, the solubility of CO in hydrocarbons (*n*-hexane, *n*-octane, *n*-hexadecane, cyclohexane, toluene, and 1-methylnaphthalene), petroleum distillates, and residues from Canadian oil sand bitumen was measured at different temperatures and pressures. The dispersion behavior of CO in different molecules was simulated by the molecular dynamics calculation. The role of water on CO dispersion in these systems was also explored. Experimental data show that the increase of both paraffinic chain length and aromaticity of molecules could hinder the dissolution of CO. By theoretical calculation, it is found that *n*-hexadecane and 1-methylnaphthalene present the strongest self-aggregation tendency, resulting in the low interaction with CO. The intermolecular forces of hydrocarbons appear to be the key factor determining the CO solubility. The dissolved H₂O molecules could weaken the intermolecular forces of hydrocarbons and thus increase the CO solubility. Based on the model system study, the solubility of CO in complex petroleum distillates and heavy residues is rationalized by their molecular composition, which is mainly dependent on the relative proportion of paraffins to aromatics.



1. INTRODUCTION

The extremely high viscosity and low mobility of heavy oil make it unable to be transported by pipeline or shipment and pose great challenges to the refining process.¹ As the petroleum supply is becoming heavier and inferior, reducing the viscosity of heavy oil has been a hot spot in both upstream and downstream petroleum industry. Partial upgrading has achieved great attention due to its low capital and operation cost, as well as potentiality to reduce the amount of diluents during the dilution process and avoid high-cost full upgrading.² When the exploited heavy oil is presented as emulsions through hot water extraction or steam injection, further demulsification and water/oil separation are needed prior to partial upgrading.³ Ng and her research group have proposed a single-stage process coupling the emulsion separation and partial upgrading by capturing the highly active in situ hydrogen produced from the water–gas shift reaction (WGSR).^{4–6} This novel process is of great interest for a more efficient and economical partial upgrading of heavy oil.

Typically, heavy oil upgrading with CO and water involves the liquid oil phase, liquid water phase, gas phase, and solid catalyst phase. This could lead to high interphase mass transfer resistance.⁷ As illustrated in Figure 1, it can be expected that the WGSR occurring in the heavy oil phase would benefit the efficient transferring of in situ hydrogen to heavy oil molecules to some extent. Generally, the molar amount of CO is far lower than that of water, indicating that CO acts as the reactant

controlling the rate of WGSR. Therefore, knowledge of the solubility of CO in heavy oil and its fractions is crucial for analyzing the efficiency of in situ hydrogen usage. Additionally, the solubility data are particularly important for understanding the phase equilibrium, establishing the kinetic model of WGSR and hydrogenation, as well as designing and optimizing the upgrading process.⁸

The solubility information of CO in model hydrocarbons is available in the field of Fischer–Tropsch synthesis.⁹ Srivatsan et al.¹⁰ and Gao et al.¹¹ have measured the solubility of CO in heavy normal paraffins. Park et al.¹² and Jáuregui-Haza et al.¹³ reported the solubility data of CO in aromatic hydrocarbons. For CO in cyclohexane, the solubility could be found in the study by Gao et al.¹⁴ The CO solubility experimental measurement in complex heavy oils and heavy fractions is scarcely reported compared with that in model compounds and light fractions. This could be challenging due to their high viscosity and thermal instability at elevated temperatures and pressures as

Received: June 10, 2021

Accepted: August 9, 2021

Published: September 1, 2021



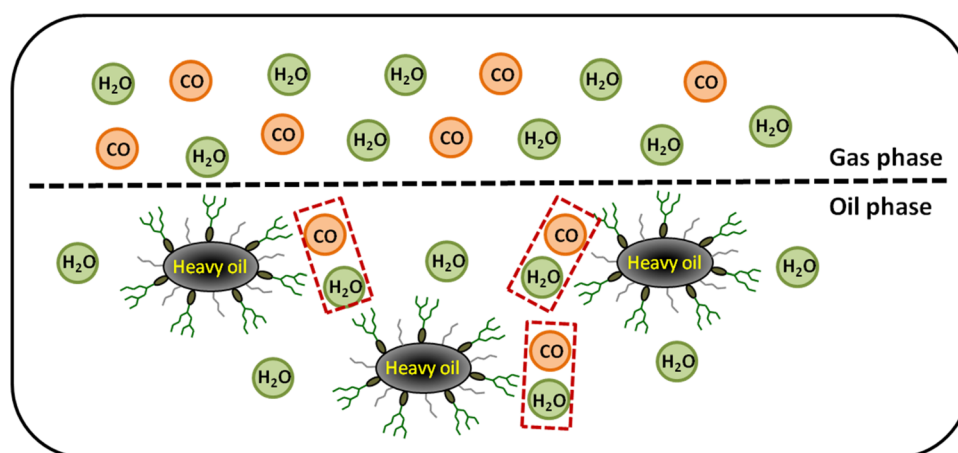


Figure 1. Phase analysis in heavy oil upgrading with CO and water.

Table 1. Specifications of the Chemicals Used in This Work

chemical name	molecular formula	CAS no.	purity provided by the supplier (mass fraction)	source
<i>n</i> -hexane	C ₆ H ₁₄	110-54-3	99.7%	Xilong Chemical Co., Ltd., China
<i>n</i> -octane	C ₈ H ₁₈	111-65-9	99.7%	Xilong Chemical Co., Ltd., China
<i>n</i> -hexadecane	C ₁₆ H ₃₄	544-76-3	99.7%	Xilong Chemical Co., Ltd., China
cyclohexane	C ₆ H ₁₂	110-82-7	99.7%	Xilong Chemical Co., Ltd., China
toluene	C ₇ H ₈	108-88-3	99.7%	Xilong Chemical Co., Ltd., China
1-methylnaphthalene	C ₁₁ H ₁₀	90-12-0	99.7%	Xilong Chemical Co., Ltd., China
carbon monoxide	CO	630-08-0	99.99%	Tianyuan Gas Manufacturing Co., Ltd., China

well as a lack of an accurate and simple determination method.¹⁵ It is the same case for hydrogen solubility measurement in heavy oil.^{16–19} Wang and his group have developed a modified direct method to measure hydrogen solubility and have successfully applied it in heavy residues, which provided an efficient method to measure CO solubility in heavy oils.²⁰ Most of the previous researches mainly aimed at the experimental measurement and predictive model development for solubility estimation.^{9–14,21,22} There is still a lack of systematic study to deal with the influence of intrinsic structures on the CO dissolving behavior at the molecular level. In recent years, molecular dynamics simulation has been an important technique to explore the microdiffusion behavior of gases in liquids.^{23–26} By combining the experimental study and molecular dynamics simulation, the effect of underlying fundamental interactions on the macroscopic dispersion property of CO in different molecules can be explored. On these bases, the solubility of CO in different complex heavy oils could be better understood.

In this work, the solubility of CO in different alkanes, cycloalkanes, and aromatics at different temperatures and pressures is measured by the modified method previously reported.²⁰ The influence of molecular structures on CO solubility is explained by the molecular dynamics simulation. Finally, the CO solubility in different heavy oil distillates and residues is then examined and discussed in terms of the molecular structures. The effect of water on the CO solubility in hydrocarbons and complex heavy oil fractions is also explored.

2. EXPERIMENTAL SECTION

2.1. Materials. The description of the chemicals, including chemical names, molecular formula, CAS registry number, purity, and chemical source of the supplier, is summarized in Table 1. Different distillates and heavy residues were separated from Canadian oil sand bitumen (a typical heavy oil, HO) by

true boiling point distillation, including gasoline (bp < 453 K, FA), diesel (bp 453–623 K, FB), vacuum gas oil (bp 623–693 K, FC), atmospheric residue (bp > 623 K, AR), and vacuum residue (bp > 693 K, VR). Main properties of these heavy oil fractions were listed in Table 2. The density was measured with a pycnometer at 293 K. The viscosity was measured using a capillary tube viscometer at 323 and 393 K. Determination of the average molecular weight was conducted on a Knauer K-7000 vapor-pressure osmometer. Elemental composition was determined using a Vario EL III elemental analyzer from Elementar Company. The SARA analysis was performed by the method described in previous literature.²⁷ The hydrocarbon analysis of FA was finished by a CP-3800 GC equipment, while that of FB and FC was obtained using an Agilent 7890B-5977 GC equipment.

2.2. Measurement of CO Solubility in Feedstocks. The solubility of CO was measured in the modified apparatus previously reported by Ji et al.,²⁰ which is briefly described here. About 80 g of degassed feed liquid was loaded into a 300 mL autoclave. After purging with CO three times to remove air as much as possible, the autoclave was heated to the given temperature and charged with a certain pressure of CO. Then, stirring was carried out and the pressure started to drop due to the diffusion of CO into the liquids. Due to the high viscosity of heavy residue, when measuring the CO solubility, the mixture of heavy residue and water was stirred for an adequate time (about 1 h) at the given temperature. The pressure in the autoclave was monitored in real time using the pressure gauge with a precision of ±0.001 MPa. When the pressure became unchanged, the stirring was stopped and the autoclave was allowed to stand still for an adequate time to ensure that the bubbles escaped completely. In this case, the equilibrium was established. Subsequently, about 2 g of the sample was taken into the sampling flask. The dissolved CO would escape out and pressurize the

Table 2. Main Properties of the Feed Heavy Oil Fractions

sample	FA ^a	FB ^b	FC ^c	HO ^d	AR ^e	VR ^f
density at 293 K, g/cm ³	0.7118	0.8916	0.9566	1.008	1.009	1.013
viscosity at 323 K, mm ² /s	1.68	5.19	41.8			
viscosity at 393 K, mm ² /s				122	523	5322
molecular weight, g/mol	232	283	319	520	782	1403
Elemental analysis						
C, wt %	85.68	85.74	85.81	84.02	83.66	84.87
H, wt %	12.78	12.65	11.66	10.42	10.39	10.18
S, wt %	1.24	1.48	2.32	4.86	5.12	4.02
N, wt %	0.06	0.09	0.10	0.38	0.63	0.81
O, wt % ^g	0.24	0.04	0.11	0.32	0.20	0.12
H/C atomic ratio	1.79	1.77	1.63	1.51	1.49	1.44
SARA composition						
saturates, wt %			64.86	35.12	25.26	19.35
aromatics, wt %			34.70	40.81	40.23	38.99
resins, wt %			0.44	21.51	25.82	29.67
asphaltenes, wt %			0	2.56	8.69	11.99

^aGasoline (bp < 453 K). ^bDiesel (bp 453–623 K). ^cVacuum gas oil (bp 623–693 K). ^dTypical heavy oil (Canadian oil sand bitumen). ^eAtmospheric residue (bp > 623 K). ^fVacuum residue (bp > 693 K). ^gThe oxygen content is obtained by the subtraction method.

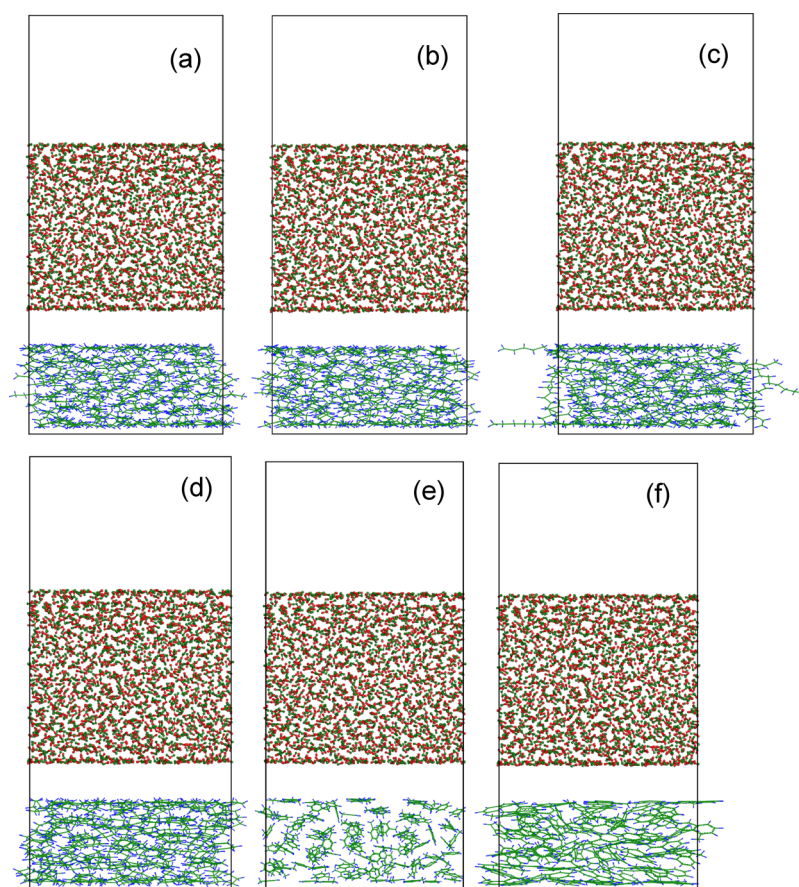


Figure 2. Simulation snapshots of CO–hydrocarbon systems. (a) 107 *n*-hexane, (b) 65 *n*-octane, (c) 41 *n*-hexadecane, (d) 110 cyclohexane, (e) 100 toluene, and (f) 65 1-methylnaphthalene.

distilled water from the surge flask into the volumetric cylinder. When the sampling flask was cooled to room temperature, the volume change of the water in the volumetric cylinder was obtained by adjusting the liquid levels in the measure system. The volume of CO dissolved in the sample could be calculated after deducting the volume of the liquid sample. Taking CO as an ideal gas, the solubility of CO can be obtained based on the state equation. The vapor pressure of feed

liquids was simultaneously measured to estimate the partial pressure of CO during the procedure, referenced from Ji et al.²⁰

The measurement accuracy of CO solubility in model compounds was evaluated by comparing the result in ethanol with the available data reported by previous researchers.²¹ Results were shown as supporting information in Figure S1. It can be seen that the solubility of CO in ethanol by the modified method agrees well with the data in the literature with a

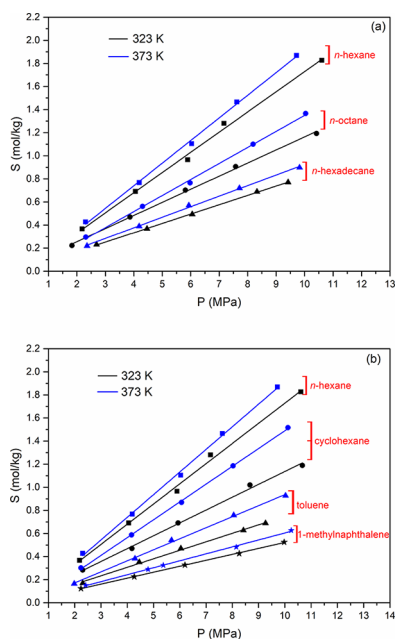


Figure 3. Solubility of CO versus pressure in model hydrocarbons at 323 and 373 K. (a) *n*-hexane, *n*-octane, and *n*-hexadecane and (b) *n*-hexane, cyclohexane, toluene, and 1-methylnaphthalene.

deviation within $\pm 5\%$. The CO solubility in selected model hydrocarbons was measured at least three times, and the error is limited to within $\pm 5\%$. The standard deviation in complicated heavy oil fractions has been presented along with the data.

2.3. Molecular Simulation Method. In this work, molecular dynamics simulations were performed using the Material Studio 7.0 simulation package. First, the molecules of CO and hydrocarbons were constructed and then the Forcite geometry optimization was carried out. The Smart algorithm was set for the preliminary optimization step. Second, the molecular boxes of 2000 CO and certain numbers of different

hydrocarbons with the same mass were created by the amorphous cell. The size of the boxes was dependent on the number of molecules. Then, the simulation box of CO molecules and that of hydrocarbon molecules were placed in the same simulated space with a thickness of 20 Å, and a certain vacuum lamella with a thickness of 5 Å was set between them, as shown in Figure 2. These systems were subsequently subjected to energy minimization by Forcite geometry optimization to get a stable structure. The algorithm was set to be the steepest descent method. The optimized systems were equilibrated in NVT simulation and NPT simulation successively. The NHL thermostat and Berendsen barostat were applied to control the temperature of NVT simulation and the pressure of NPT simulation with random initial velocities and a time step of 1.0 fs. The total time of NVT simulation and that of NPT simulation were 100 and 300 ps, respectively. The force field was selected as COMPASS, and the summation method was set to be the Ewald model. The variations of energies and temperature versus time during NVT and NPT simulation for the systems in the present work indicate that the energies during NVT simulation vary within ± 100 kcal/mol while the temperature during NPT simulation varies within ± 10 K, which means that the simulations have been equilibrated. The typical result for the 2000 CO + 107 *n*-hexane system versus time is shown in Figure S2 as supporting information.

3. RESULTS AND DISCUSSION

3.1. CO Dissolution in Different Hydrocarbons. Figure 3 shows the solubility of CO (*S*) dissolved in model hydrocarbons with the change of pressure (*P*) at 323 and 373 K. It is obvious that the solubility of CO in alkanes, cycloalkanes, and aromatics increases linearly with the pressure increasing. The high temperature also facilitates the dissolution of CO. The rise of solubility with pressure is faster at a relatively higher temperature. The dissolution of CO implies the intermolecular interaction of CO with hydrocarbons. Since the CO molecule has a low dipole moment of 0.10, the main van der Waals force

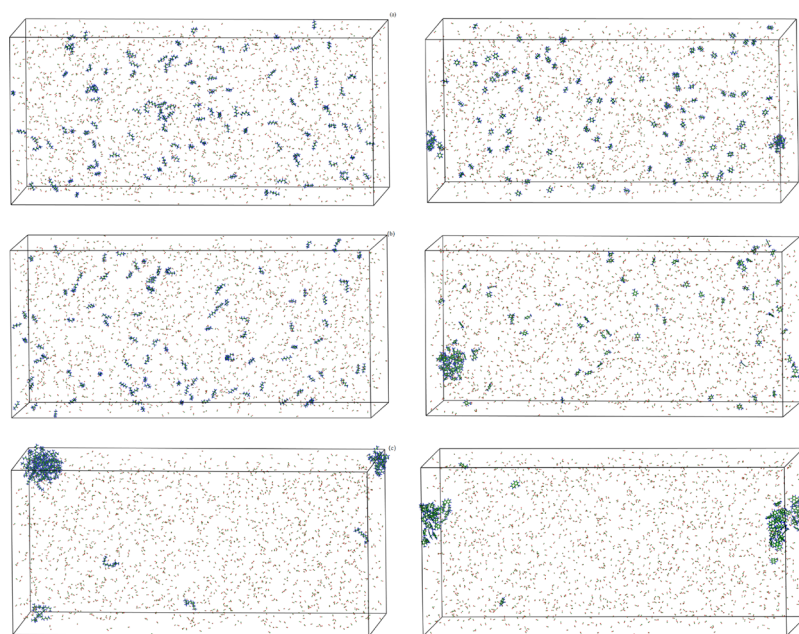


Figure 4. The simulated configurations of 2000 CO molecules and certain numbers of hydrocarbons. (a) 107 *n*-hexane, (b) 65 *n*-octane, (c) 41 *n*-hexadecane, (d) 110 cyclohexane, (e) 100 toluene, and (f) 65 1-methylnaphthalene.

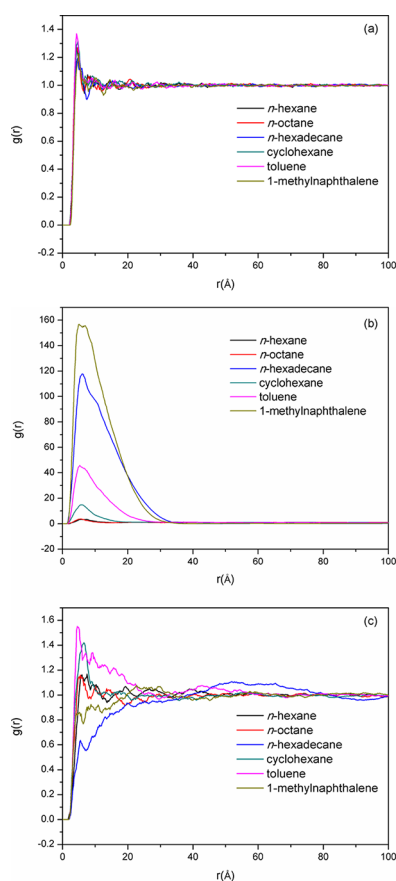


Figure 5. RDF of different molecules at 300 K and 1 MPa. (a) CO–CO molecules, (b) hydrocarbon–hydrocarbon molecules, and (c) CO–hydrocarbon molecules.

within hydrocarbon molecules, CO molecules, and between hydrocarbon and CO molecules is the London force. High pressure could decrease the distance between hydrocarbon and CO molecules, resulting in stronger London force, as stated by Yang et al.^{28–31} When more CO molecules are pushed into the hydrocarbons, the distance within hydrocarbon molecules can be increased and weaker London force can be expected, which benefits CO molecules to get into the liquid phase. Consequently, a higher solubility is observed at a higher pressure. As temperature increases, the increased distance between CO and hydrocarbon molecules could block the diffusion of CO, while the increased distance within hydrocarbon molecules could favor the intramolecular interaction of CO. Unlike CO₂ dissolution in organic liquids,^{28–31} the positive role of temperature appears to exceed the negative one for CO dissolution.

Under the same conditions, the solubility of CO in *n*-alkanes decreases with the length of carbon chain increases. This suggests that the long paraffinic side chain hinders the intramolecular interactions with CO. The solubility of CO decreases in the order of *n*-hexane > cyclohexane > toluene > 1-methylnaphthalene. It indicates that the solubility of CO in aromatics tends to be lower than that in naphthenic and paraffinic hydrocarbons. Furthermore, a rise of the aromaticity of hydrocarbons restrains the dissolution of CO. The effect of pressure on the solubility of CO in *n*-alkanes with a smaller carbon number is much stronger.

To further reveal the relationship between the inherent molecular structures of hydrocarbons and the CO solubility, the dispersion property of CO in hydrocarbons was tentatively studied through a molecular dynamics simulation approach.

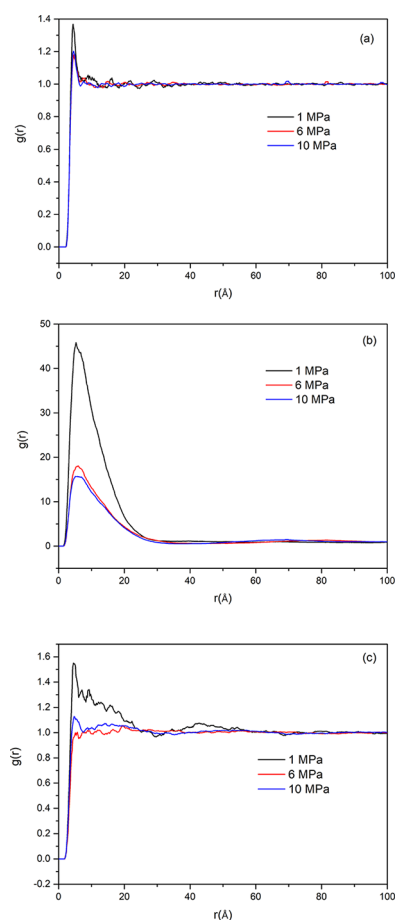


Figure 6. RDF of molecules in toluene + CO at 300 K under different pressures. (a) CO–CO molecules, (b) toluene–toluene molecules, and (c) CO–toluene molecules.

Figure 4 displays the simulated configurations of 2000 CO molecules and certain numbers of hydrocarbons with the same mass. Results show that CO molecules diffuse sufficiently in *n*-hexane and *n*-octane. Meanwhile, *n*-hexadecane exhibits aggregated structures in the CO + *n*-hexadecane system obviously. This could be rationalized by the stronger London forces of linear alkane molecules with longer alkyl chains.²⁹ In contrast, cyclohexane molecule with the shape of a chair or boat and aromatic molecules with a ring show a larger surface area of contact than the linear alkane molecules. Meanwhile, the polarizability of cyclohexane and aromatics is stronger. Therefore, the London forces within cyclohexane and aromatics are stronger.²⁸ This is the reason why an obvious aggregation behavior can also be observed for the aromatics and tends to be more distinct as the aromaticity becomes much higher. It clearly indicates that the diffusion of CO is restricted by the hydrocarbon molecules with longer alkyl side chains and higher aromatic moieties, which is well supported by the above solubility measurements.

Figure 5 shows the radial distribution function (RDF) of CO–CO molecules, hydrocarbon–hydrocarbon molecules, and CO–hydrocarbon molecules at 300 K and 1 MPa. A peak of RDF of CO–CO molecules lower than 1.3 is found at a radius (*r*) of about 0.50 nm that is slightly higher than the diameters of CO molecules. This suggests the CO molecules are shown as aggregates with a very low aggregation degree in CO + hydrocarbons systems. The RDF of hydrocarbon–hydrocarbon

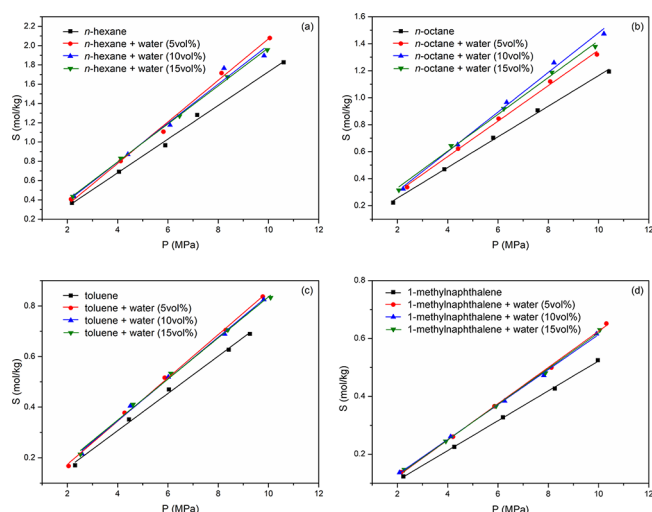


Figure 7. Solubility of CO versus pressure in model compounds with different amounts of water at 323 K. (a) *n*-hexane, (b) *n*-octane, (c) toluene, and (d) 1-methylnaphthalene.

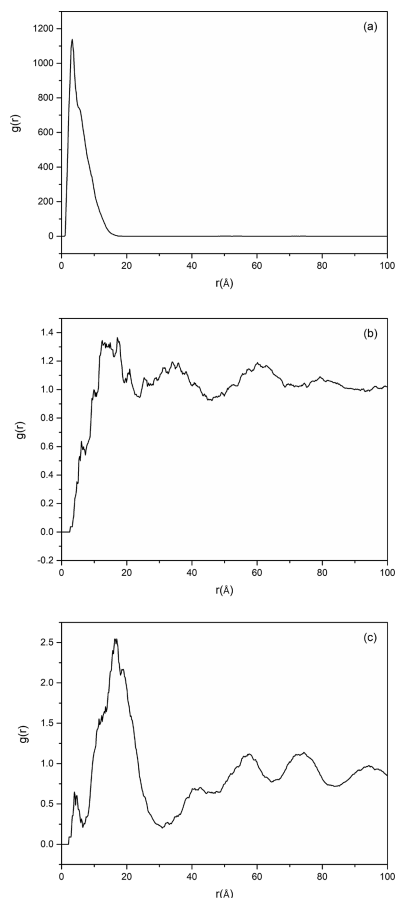


Figure 8. RDF of molecules in *n*-hexane + CO + water at 300 K. (a) H₂O–H₂O molecules, (b) CO–H₂O molecules, and (c) *n*-hexane–H₂O molecules.

molecules displays a distinct peak at r of around 0.55 nm, indicating that the hydrocarbon molecules are strongly aggregated. *n*-Hexane and *n*-octane present the lowest aggregation degree, while the aggregation of *n*-hexadecane and 1-methylnaphthalene is strongest, consistent with the London forces within these molecules. The aggregation behavior could prevent CO

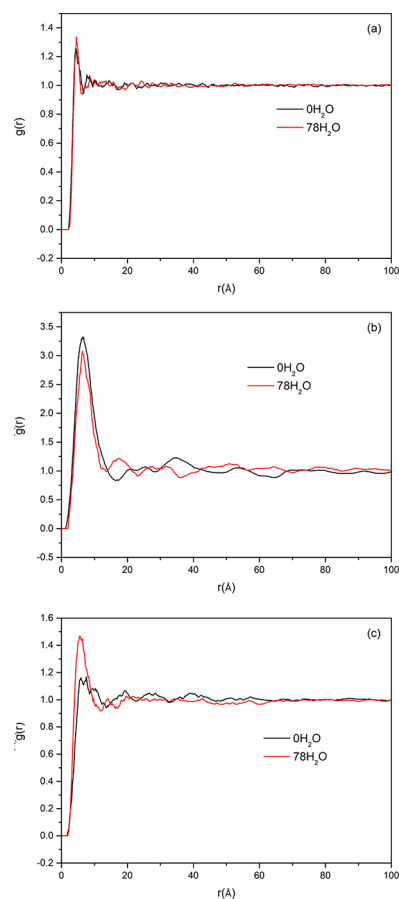


Figure 9. RDF of molecules in *n*-hexane + CO + water at 300 K. (a) CO–CO molecules, (b) *n*-hexane–*n*-hexane molecules, and (c) CO–*n*-hexane molecules.

molecules from interacting with hydrocarbon molecules. The RDF of CO–*n*-hexadecane and CO–1-methylnaphthalene molecules shows no peak, which further confirms that the interaction between CO and these two hydrocarbons is relatively weaker.

Figure 6 shows the RDF of CO–CO molecules, hydrocarbon–hydrocarbon molecules, and CO–hydrocarbon molecules at 300 K under different pressures for the CO + toluene system. The corresponding results for other CO + hydrocarbon systems are presented in Figures S3, S4, and S5 as supporting information. As can be seen, the RDF of CO–CO molecules, toluene–toluene, and CO–toluene decreases with pressure increasing, among which the decrease of the RDF of toluene–toluene molecules is the most significant. It indicates that the aggregation of molecules is impeded by high pressure. When more CO molecules are pushed into the toluene molecules, the self-aggregates of toluene molecules are remarkably disintegrated, which can conversely facilitate the CO dissolution. The same tendency can be observed for *n*-octane, *n*-hexadecane, cyclohexane, and 1-methylnaphthalene. It appears that the self-aggregation of *n*-hexane molecules is little affected by altering the pressure. This could be attributed to its low self-aggregation degree and the limitation of pressure effect. On the whole, for CO + hydrocarbon systems, it is the CO molecules that disperse in the hydrocarbon molecular aggregates. The aggregation property of hydrocarbon molecules appears to be the key factor determining the CO solubility.

3.2. Role of Water in CO Dissolution in Model Hydrocarbons. Figure 7 shows the solubility of CO in different

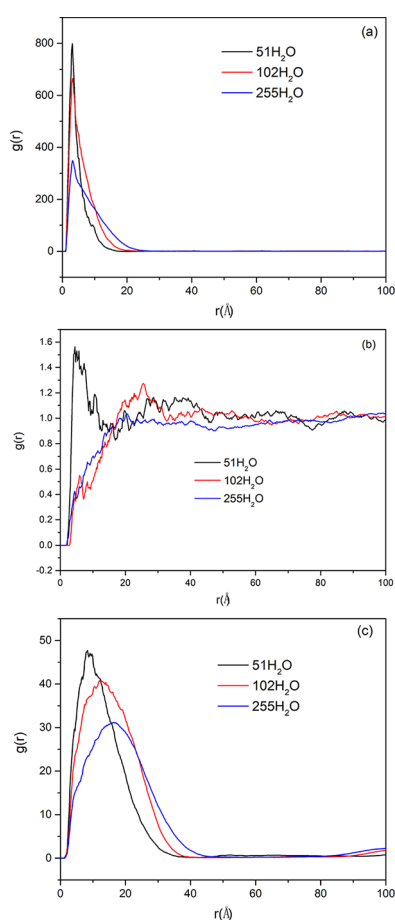


Figure 10. RDF of molecules in 1-methylnaphthalene + CO + water at 300 K. (a) 1-methylnaphthalene–H₂O molecules, (b) CO–H₂O molecules, and (c) H₂O–H₂O molecules.

hydrocarbons at 323 K with different amounts of water. As can be seen, there is an apparent increase of CO solubility when water is added into the hydrocarbon. Since the solubility of CO in water is much lower, this result implies that there is synergism on CO dissolution between hydrocarbon and water.³² The synergism is not shown to be promoted with more water added, which might be restricted by the solubility of water in hydrocarbons. It can be inferred that the synergism could be mainly ascribed to the dissolved water in the hydrocarbons. The same observation has also been reported by Karandikar et al.³³ The above results suggest that the water in the exploited oil benefits the dissolution of CO during thermal upgrading under CO/syngas and water.

The effect of water on the dispersion property of CO in *n*-hexane and 1-methylnaphthalene is further studied by molecular dynamics simulation. The number of H₂O molecules was determined to be 78 based on the 15 wt % of the 107 *n*-hexane. Figure 8 displays the RDF of H₂O–H₂O molecules, CO–H₂O molecules, and *n*-hexane–H₂O molecules in the CO + *n*-hexane + water system. The corresponding RDF of CO–CO molecules, *n*-hexane–*n*-hexane molecules, and CO–*n*-hexane molecules is shown in Figure 9. As can be seen from the sharp peak of the RDF of H₂O–H₂O molecules, H₂O molecules are strongly aggregated with each other due to the high van der Waals forces (mainly dipole–dipole force) and hydrogen bonding forces. There is no obvious aggregation of H₂O molecules with CO molecules, suggesting a low interaction between them.

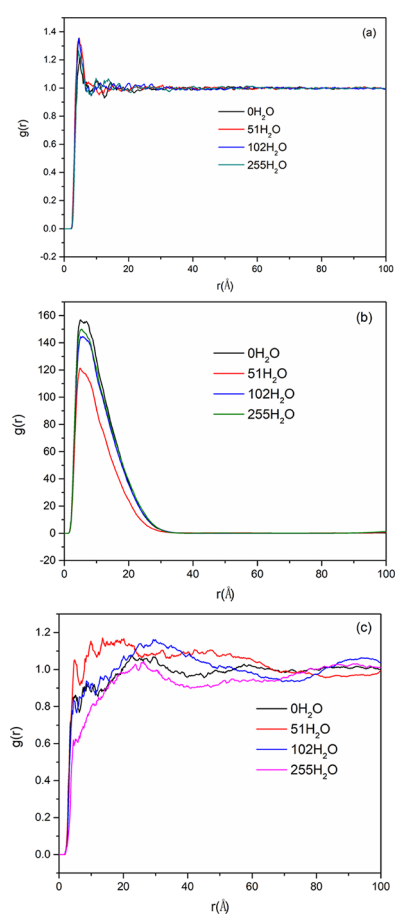


Figure 11. RDF of molecules in 1-methylnaphthalene + CO + water at 300 K. (a) CO–CO molecules, (b) 1-methylnaphthalene–1-methylnaphthalene molecules, and (c) CO–1-methylnaphthalene molecules.

Thereby, the addition of H₂O molecules has little effect on the weak aggregation of CO molecules. In contrast, a peak of RDF of *n*-hexane–H₂O molecules around 2.5 is observed, which means that H₂O molecules are aggregated with *n*-hexane molecules. It can be expected that the self-aggregation of *n*-hexane molecules is weakened by H₂O molecules, which is well demonstrated by the decline of the peak of RDF of *n*-hexane–*n*-hexane molecules. As a consequence, the interaction of CO with *n*-hexane can be improved, as evidenced by the obvious increase of the peak value of RDF of CO–*n*-hexane molecules. Correspondingly, the CO solubility is increased by the addition of water.

The variation of CO dispersion in 1-methylnaphthalene with different numbers of H₂O molecules is also studied. The number of H₂O molecules was determined to be 51, 102, and 255 based on the 10, 20, and 50 wt % of the 65 1-methylnaphthalene. Figure 10 shows the RDF of H₂O–H₂O molecules, CO–H₂O molecules, and 1-methylnaphthalene–H₂O molecules. The corresponding RDF of CO–CO molecules, 1-methylnaphthalene–1-methylnaphthalene molecules, and CO–1-methylnaphthalene molecules is presented in Figure 11. The same trend can be found for the role of water on the dispersion of CO in 1-methylnaphthalene as that in *n*-hexane, which mainly lies in the breakage of 1-methylnaphthalene self-aggregates. When more H₂O molecules exist, the peak of RDF of 1-methylnaphthalene–H₂O molecules is reduced significantly. The position of the peak is shifted to the higher part, indicating that the 1-methylnaphthalene–H₂O aggregate becomes larger. This can be rationalized

Table 3. Solubility of CO in Heavy Oil Distillates

T (K)	FA ^a		FB ^b		FC ^c	
	P (MPa)	S (mol/kg)	P (MPa)	S (mol/kg)	P (MPa)	S (mol/kg)
323	2.17	0.2286 ± 0.0160	2.04	0.1151 ± 0.0030	2.43	0.1089 ± 0.0020
	4.25	0.4260 ± 0.0036	4.18	0.2368 ± 0.0118	4.23	0.1897 ± 0.0064
	6.09	0.5646 ± 0.0059	5.93	0.3370 ± 0.0210	6.32	0.2838 ± 0.0052
	8.15	0.7249 ± 0.0035	8.32	0.4764 ± 0.0181	8.16	0.3763 ± 0.0095
	10.0	0.9138 ± 0.0126	9.80	0.5787 ± 0.0248	10.0	0.4711 ± 0.0093
373	2.04	0.2475 ± 0.0158	2.53	0.1537 ± 0.0033	2.16	0.1158 ± 0.0047
	4.06	0.4869 ± 0.0082	4.14	0.2532 ± 0.0120	4.22	0.2432 ± 0.0129
	6.02	0.7033 ± 0.0164	6.16	0.3839 ± 0.0019	5.77	0.3279 ± 0.0004
	8.25	0.9755 ± 0.0139	8.25	0.5278 ± 0.0002	8.09	0.4584 ± 0.0270
	9.76	1.125 ± 0.0363	10.1	0.6428 ± 0.0255	10.4	0.6110 ± 0.0167
423	2.43	0.3276 ± 0.0042	2.25	0.1493 ± 0.0038	2.27	0.1323 ± 0.0013
	4.39	0.5824 ± 0.0159	4.20	0.2840 ± 0.0015	3.99	0.2464 ± 0.0091
	6.23	0.8117 ± 0.0193	6.13	0.4275 ± 0.0023	5.91	0.3651 ± 0.0034
	8.16	1.060 ± 0.0455	8.32	0.5773 ± 0.0167	8.02	0.4936 ± 0.0126
	9.96	1.334 ± 0.0311	9.89	0.6965 ± 0.0216	9.89	0.6251 ± 0.0042

^aGasoline (bp < 453 K). ^bDiesel (bp 453–623 K). ^cVacuum gas oil (bp 623–693 K).

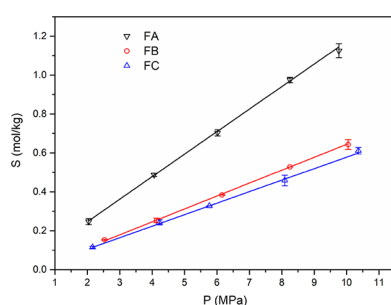


Figure 12. Solubility of CO in heavy oil distillates versus pressure at 373 K.

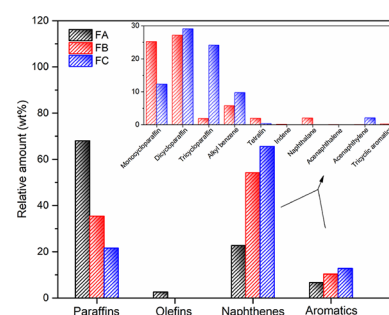


Figure 13. Hydrocarbon composition of FA, FB, and FC.

by the larger aggregates of H₂O–H₂O molecules. It can be predicted that the weakening effect of H₂O molecules on 1-methylnaphthalene self-aggregation becomes lower gradually, as proved by the increase of RDF of 1-methylnaphthalene–1-methylnaphthalene molecules with a greater number of H₂O molecules added. The interaction of CO with H₂O and 1-methylnaphthalene is still low. Overall, it is concluded that the promotion of H₂O on CO dispersion in hydrocarbon mainly originates from the strong interaction of the H₂O aggregate with the hydrocarbon molecule aggregate.

3.3. CO Dissolution in Heavy Oil Fractions. The solubility of CO in FA, FB, and FC from Canadian oil sand bitumen was measured at temperatures from 323 to 423 K and pressures up to 10 MPa. The data are listed in Table 3. Consistent with the analysis result by model compounds, the solubility in these heavy oil fractions increases with pressure and temperature increasing. The variation of solubility as a function of pressure at 423 K is depicted in Figure 12 as an example. Under the same experimental conditions, the solubility of CO follows the order of FA > FB > FC. The solubility of CO in FA is extremely higher than the others. As seen from Table 2, FA presents the highest H/C atomic ratio and lowest molecular weight. It indicates that FA is the least aromatic fraction. This is in good agreement with the hydrocarbon composition of these fractions as shown in Figure 13. The paraffin and naphthene contents in FA can be as high as 68 and 23 wt %, respectively, while the portion of aromatics is only 6.7 wt %. Since the paraffins and naphthenes facilitate the diffusion of CO, their high

amount could significantly contribute to the high solubility of CO in FA. FB comprises more paraffins and naphthenes than FC, which could improve the CO dissolution. Meanwhile, the aromatic hydrocarbons in FC are of higher amount and more condensed than those in FB. This could hinder the CO dissolution in FC. During the partial upgrading process with CO and water, the increase of CO solubility can be expected as the hydrogenation of heavy oil proceeds.

The solubility of Canadian oil sand bitumen and that of its residues were simultaneously measured at temperatures ranging from 473 to 573 K and pressure up to 10 MPa, with results shown in Table 4. Figure 14 compares the solubility of CO in these feedstocks and FC as a function of pressure at 473 K. Results indicate that the order of CO solubility is FC > HO > AR > VR. This can be attributed to the decrease of the amount of saturates when the boiling range of heavy oil becomes higher. The ratio of saturates to aromatic fractions has decreased from 1.85 for FC to 0.54 for HO and even 0.24 for VR. The extensive aromatic structures mainly restrict the interaction between CO molecules and heavy residue molecules. Due to the presence of light distillates, heavy crude oil performs the highest solubility of CO. It can be inferred that recycling certain heavy oil fractions could improve the solubility of CO. Furthermore, these heavy oil fractions contain a portion of nitrogen, sulfur, and oxygen as shown in Table 2. The heteroatoms could contribute to the intermolecular forces of molecules by altering the polarizability and distortability and definitely affect the CO solubility. According to the present study, it seems that the solubility of CO in different

Table 4. Solubility of CO in Heavy Oil and Its Residues

T (K)	HO ^a		AR ^b		VR ^c	
	P (MPa)	S (mol/kg)	P (MPa)	S (mol/kg)	P (MPa)	S (mol/kg)
473	2.05	0.1191 ± 0.0141	2.24	0.0858 ± 0.0081	1.93	0.0529 ± 0.0121
	4.14	0.2401 ± 0.0181	4.28	0.1552 ± 0.0121	4.53	0.1135 ± 0.0115
	6.18	0.3577 ± 0.0231	6.23	0.2239 ± 0.0053	6.31	0.1581 ± 0.0224
	8.31	0.4758 ± 0.0378	8.25	0.2974 ± 0.0060	7.96	0.1977 ± 0.0185
	9.98	0.5809 ± 0.0313	9.94	0.3573 ± 0.0120	10.2	0.2519 ± 0.0256
523	2.21	0.1586 ± 0.0095	2.27	0.0964 ± 0.0032	2.15	0.0813 ± 0.0087
	4.16	0.3021 ± 0.0193	4.31	0.1804 ± 0.0077	4.20	0.1425 ± 0.0126
	5.94	0.4423 ± 0.0198	6.35	0.2681 ± 0.0135	6.04	0.2087 ± 0.0157
	8.12	0.6048 ± 0.0222	8.17	0.3387 ± 0.0207	8.05	0.2808 ± 0.0272
	10.1	0.7573 ± 0.0384	10.1	0.4133 ± 0.0215	10.1	0.3492 ± 0.0302
573 K	2.01	0.1671 ± 0.0130	2.22	0.1286 ± 0.0054	2.21	0.0971 ± 0.0102
	3.98	0.3307 ± 0.0154	4.32	0.2565 ± 0.0074	4.02	0.1693 ± 0.0147
	6.04	0.5012 ± 0.0201	6.20	0.3723 ± 0.0208	5.94	0.2465 ± 0.0230
	8.02	0.6542 ± 0.0185	8.15	0.4961 ± 0.0268	8.10	0.3181 ± 0.0196
	10.0	0.8334 ± 0.0237	10.0	0.6088 ± 0.0170	10.4	0.4008 ± 0.0225

^aTypical heavy oil (Canadian oil sand bitumen). ^bAtmospheric residue (bp > 623 K). ^cVacuum residue (bp > 693 K).

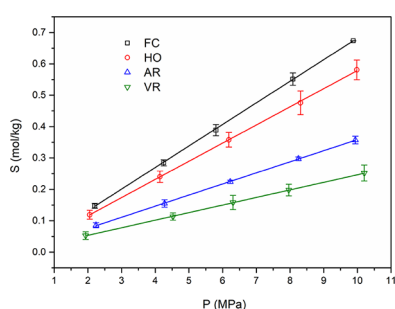


Figure 14. Solubility of CO in heavy crude oil and its residues versus pressure at 473 K.

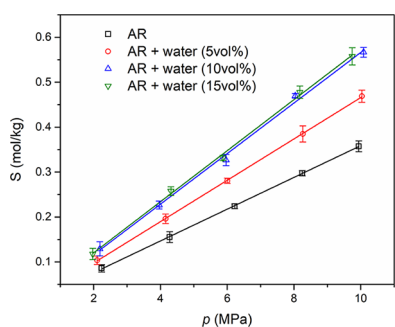


Figure 15. Solubility of CO in atmospheric residues with different amounts of water versus pressure at 473 K.

heavy oil fractions can be simply compared by analyzing the group or hydrocarbon-class composition. In addition, the partial upgrading of heavy oil with CO and water involved the solid catalyst phase. As studied by Cai et al.,³⁴ the different solid additives including hydrotreating catalysts could raise the apparent solubility of hydrogen in petroleum fractions. Therefore, the impact of solid additives is worth studying in future works to enhance the CO dispersion and dissolution. Figure 15 shows the effect of water on the solubility of CO in AR at 473 K. It can be clearly seen that water could promote the CO dissolution in AR. The extent of promotion might be limited by the solubility of water in AR, indicating that the soluble water in AR is the promoter for CO dissolution.

4. CONCLUSIONS

The structure–solubility relationship of CO dispersion in organic liquids was explored. The dispersion behavior of CO in different molecules was simulated by the molecular dynamics calculation. The role of water on CO dispersion in these systems was also studied. Experimental data show that the increase of both paraffinic chain length and aromaticity of molecules could hinder the dissolution of CO. By theoretical calculation, it is found that *n*-hexadecane and 1-methylnaphthalene present the strongest self-aggregation tendency, resulting in the low interaction with CO. The intermolecular forces of hydrocarbons appear to be the key factor determining the CO solubility. The dissolved H₂O molecules could weaken the intermolecular forces of hydrocarbons and thus increase the CO solubility. Based on the model system study, the solubility of CO in complex petroleum distillates and heavy residues is rationalized by their molecular composition, which is mainly dependent on the relative proportion of paraffins to aromatics.

ASSOCIATED CONTENT

Supporting Information

The Supporting Information is available free of charge at <https://pubs.acs.org/doi/10.1021/acsomega.1c03060>.

The CO solubility in ethanol (Figure S1); the variation of energies and temperatures during 100 ps NVT and 300 ps NPT simulation for the 2000 CO + 107 *n*-hexane system. (Figure S2); the RDF of CO–CO molecules for different hydrocarbon + CO systems at 300 K under different pressures (Figure S3); the RDF of hydrocarbon–hydrocarbon molecules for different hydrocarbon + CO systems at 300 K under different pressures (Figure S4); and the RDF of CO–hydrocarbon molecules for different hydrocarbon + CO systems at 300 K under different pressures (Figure S5) (PDF)

AUTHOR INFORMATION

Corresponding Author

He Liu – State Key Laboratory of Heavy Oil Processing, College of Chemical Engineering, China University of Petroleum (East China), Qingdao, Shandong 266580, China; orcid.org/0000-0002-1450-5451; Email: liuhe@upc.edu.cn

Authors

Shiguang Fan – State Key Laboratory of Heavy Oil Processing, College of Chemical Engineering, China University of Petroleum (East China), Qingdao, Shandong 266580, China; orcid.org/0000-0002-0917-6681

Jian Wang – State Key Laboratory of Heavy Oil Processing, College of Chemical Engineering, China University of Petroleum (East China), Qingdao, Shandong 266580, China; orcid.org/0000-0003-3706-4481

Hao Liu – State Key Laboratory of Heavy Oil Processing, College of Chemical Engineering, China University of Petroleum (East China), Qingdao, Shandong 266580, China

Aijun Guo – State Key Laboratory of Heavy Oil Processing, College of Chemical Engineering, China University of Petroleum (East China), Qingdao, Shandong 266580, China

Kun Chen – State Key Laboratory of Heavy Oil Processing, College of Chemical Engineering, China University of Petroleum (East China), Qingdao, Shandong 266580, China; orcid.org/0000-0002-8556-8900

Zongxian Wang – State Key Laboratory of Heavy Oil Processing, College of Chemical Engineering, China University of Petroleum (East China), Qingdao, Shandong 266580, China

Litao Wang – Petrochina Petrochemical Research Institute, Beijing 102249, China

Complete contact information is available at:

<https://pubs.acs.org/10.1021/acsomega.1c03060>

Notes

The authors declare no competing financial interest.

ACKNOWLEDGMENTS

This work was supported by the National Natural Science Foundation of China (21908248), the Fundamental Research Funds for the Central Universities (19CX02013A and 20CX02206A), the China National Petroleum Corporation (PRIKY19022), and the Development Fund of State Key Laboratory of Heavy Oil Processing.

REFERENCES

- (1) Alemán-Vázquez, L. O.; Torres-Mancerac, P.; Ancheyta, J.; Ramírez-Salgado, J. Use of hydrogen donors for partial upgrading of heavy petroleum. *Energy Fuels* **2016**, *30*, 9050–9060.
- (2) Gray, M. R. Fundamentals of partial upgrading of bitumen. *Energy Fuels* **2019**, *33*, 6843–6856.
- (3) Shu, G.; Bu, K.; Zhao, B.; Zheng, S. Separation of SAGD produced emulsions through a combined pre-dewatering and demulsification process. *J. Pet. Sci. Eng.* **2021**, *201*, 108493–108505.
- (4) Ng, F. T. T. Upgrading heavy oil/bitumen emulsions via in situ hydrogen generation. *Prepr. Symp. - Am. Chem. Soc., Div. Fuel Chem.* **1998**, *43*, 456–460.
- (5) Ng, F. T. T.; Milad, I. K. Catalytic desulphurization of benzothiophene in an emulsion via in situ generated H₂. *Appl. Catal., A* **2000**, *200*, 243–254.
- (6) Jia, L. Oil sands bitumen emulsion upgrading by using in situ hydrogen generated through the water gas shift reaction. Waterloo: University of Waterloo, 2014.
- (7) Arai, K.; Adschiri, T.; Watanabe, M. Hydrogenation of hydrocarbons through partial oxidation in supercritical water. *Ind. Eng. Chem. Res.* **2000**, *39*, 4697–4701.
- (8) Qureshi, M. S.; Le Nedelec, T.; Guerrero-Amaya, H.; Uusi-Kyyny, P.; Richon, D.; Alopaeus, V. Solubility of carbon monoxide in bio-oil compounds. *J. Chem. Thermodyn.* **2016**, *105*, 296–311.
- (9) Srinivas, S.; Field, R. P.; Watanasiri, S.; Herzog, H. J. Correlation to predict solubility of hydrogen and carbon monoxide in heavy paraffins. *Fluid Phase Equilib.* **2012**, *320*, 11–25.
- (10) Srivatsan, S.; Yi, X.; Robinson, R. L., Jr.; Gasem, K. A. M. Solubilities of carbon monoxide in heavy normal paraffins at temperatures from 311 to 423K and pressures to 10.2 MPa. *J. Chem. Eng. Data* **1995**, *40*, 237–240.
- (11) Gao, W.; Robinson, R. L.; Gasem, K. A. M. High-pressure solubilities of hydrogen, nitrogen, and carbon monoxide in dodecane from 344 to 410 K at pressures to 13.2 MPa. *J. Chem. Eng. Data* **1999**, *44*, 130–132.
- (12) Park, J.; Yi, X.; Gasem, K. A. M.; Robinson, R. L., Jr. Solubilities of carbon monoxide in aromatic hydrocarbons at temperatures from 323 to 433K and pressures to 23.3 MPa. *J. Chem. Eng. Data* **1995**, *40*, 245–247.
- (13) Jáuregui-Haza, U. J.; Pardillo-Fontdevila, E. J.; Wilhelm, A. M.; Delmas, H. Solubility of hydrogen and carbon monoxide in water and some organic solvents. *Lat. Am. Appl. Res.* **2004**, *34*, 71–74.
- (14) Gao, W.; Robinson, R. L.; Gasem, K. A. M. Solubilities of hydrogen in hexane and of carbon monoxide in cyclohexane at temperatures from 344.3 to 410.9K and pressures to 15 MPa. *J. Chem. Eng. Data* **2001**, *46*, 609–612.
- (15) Abedi, S. J.; Seyfaie, S.; Shaw, J. M. Unusual retrograde condensation and asphaltene precipitation in a model heavy oil system. *Pet. Sci. Technol.* **1998**, *16*, 209–226.
- (16) Cai, H. Y.; Shaw, J. M.; Chung, K. H. Hydrogen solubility measurements in heavy oil and bitumen cuts. *Fuel* **2001**, *80*, 1055–1063.
- (17) Baird, Z. S.; Uusi-Kyyny, P.; Oja, V.; Alopaeus, V. Hydrogen solubility of shale oil containing polar phenolic compounds. *Ind. Eng. Chem. Res.* **2017**, *56*, 8738–8747.
- (18) Nasery, S.; Barati-Harooni, A.; Tatar, A.; Najafi-Marghmaleki, A.; Mohammadi, A. H. Accurate prediction of solubility of hydrogen in heavy oil fractions. *J. Mol. Liq.* **2016**, *222*, 933–943.
- (19) Saajanlehto, M.; Uusi-Kyyny, P.; Alopaeus, V. Hydrogen solubility in heavy oil systems: Experiments and modeling. *Fuel* **2014**, *137*, 393–404.
- (20) Ji, S.; Wang, Z.; Guo, A.; Zhou, Y.; Chen, K. Determination of hydrogen solubility in heavy fractions of crude oils by a modified direct method. *J. Chem. Eng. Data* **2013**, *58*, 3453–3457.
- (21) Tonner, S. P.; Wainwright, M. S.; Trimm, D. L.; Cant, N. W. Solubility of carbon monoxide in alcohols. *J. Chem. Eng. Data* **1983**, *28*, 59–61.
- (22) Uusi-Kyyny, P.; Pakkanen, M.; Linnekoski, J.; Alopaeus, V. Hydrogen solubility measurements of analyzed tall oil fractions and a solubility model. *J. Chem. Thermodyn.* **2017**, *105*, 15–20.
- (23) Anderson, L. R.; Yang, Q.; Ediger, A. M. Comparing gas transport in three polymers via molecular dynamics simulation. *Phys. Chem. Chem. Phys.* **2018**, *20*, 22123–22133.
- (24) Yuan, H.; Gosling, C.; Kokayeff, P.; Murad, S. Prediction of hydrogen solubility in heavy hydrocarbons over a range of temperatures and pressures using molecular dynamics simulations. *Fluid Phase Equilib.* **2010**, *299*, 94–101.
- (25) Economou, I. G.; Garrido, N. M.; Makrodimitri, Z. A. Prediction of microscopic structure and physical properties of complex fluid mixtures based on molecular simulation. *Fluid Phase Equilib.* **2010**, *296*, 125–132.
- (26) Li, C.; Pu, H.; Zhong, X.; Li, Y.; Zhao, J. X. Interfacial interactions between Bakken crude oil and injected gases at reservoir temperature: A molecular dynamics simulation study. *Fuel* **2020**, *276*, 118058–118064.
- (27) Guo, A.; Wang, Z.; Zhang, H.; Zhang, X.; Wang, Z. Hydrogen transfer and coking propensity of petroleum residues under thermal processing. *Energy Fuels* **2010**, *24*, 3093–3100.
- (28) Yang, Z.; Li, M.; Peng, B.; Lin, M.; Dong, Z. Dispersion property of CO₂ in oil. 1. Volume expansion of CO₂ + alkane at near critical and supercritical condition of CO₂. *J. Chem. Eng. Data* **2012**, *57*, 882–889.
- (29) Yang, Z.; Li, M.; Peng, B.; Lin, M.; Dong, Z. Dispersion property of CO₂ in oil. 2: Volume expansion of CO₂ + organic liquid at near-

critical and supercritical conditions of CO₂. *J. Chem. Eng. Data* **2012**, *57*, 1305–1311.

(30) Yang, Z.; Li, M.; Peng, B.; Lin, M.; Dong, Z. Dispersion property of CO₂ in oil. Part 3: Aggregation of CO₂ molecule in organic liquid at near critical and supercritical condition of CO₂. *J. Dispersion Sci. Technol.* **2014**, *35*, 143–149.

(31) Yang, Z.; Li, M.; Peng, B.; Lin, M.; Dong, Z. Volume expansion of CO₂+oil at near critical and supercritical conditions of CO₂. *Fuel* **2013**, *112*, 283–288.

(32) Takahashi, M.; Kobayashi, Y.; Takeuchi, H. Diffusion coefficients and solubilities of carbon dioxide in binary mixed solvents. *J. Chem. Eng. Data* **1982**, *27*, 328–331.

(33) Karandikar, B. M.; Morsi, B. I.; Shah, Y. T.; Carr, N. L. Effect of water on the solubility and mass transfer coefficients of CO and H₂ in a Fischer-Tropsch liquid. *Chem. Eng. J.* **1986**, *33*, 157–168.

(34) Cai, H. Y.; Shaw, J. M.; Chung, K. H. The impact of solid additives on the apparent solubility of hydrogen in petroleum fractions and model hydrocarbon liquids. *Fuel* **2001**, *80*, 1065–1077.

